Available online at www.sciencedirect.com
SCIENCE DIRECT
Bioorganic & Medicinal Chemistry 14 (2006) 4055–4066
Bioorganic & Medicinal Chemistry

Synthesis, labeling, and biological evaluation of halogenated 2-quinolinecarboxamides as potential radioligands for the visualization of peripheral benzodiazepine receptors

Andrea Cappelli,[a,*] Mario Matarrese,[b] Rosa Maria Moresco,[b] Salvatore Valenti,[a] Maurizio Anzini,[a] Salvatore Vomero,[a] Elia Anna Turolla,[b] Sara Belloli,[b] Pasquale Simonelli,[b] Maria Azzurra Filannino,[b] Michela Lecchi[c] and Ferruccio Fazio[b]

[a]*Dipartimento Farmaco Chimico Tecnologico and European Research Centre for Drug Discovery and Development, Università degli Studi di Siena, Via A. Moro, 53100 Siena, Italy*
[b]*Istituto di Bioimmagini e Fisiologia Molecolare, CNR, Università di Milano/Bicocca, Istituto H. S. Raffaele, Via Olgettina 60, 20132 Milano, Italy*
[c]*Istituto di Scienze Radiologiche, Università degli Studi di Milano, Via Rudinì 8, 20142 Milano, Italy*

Received 6 December 2005; revised 1 February 2006; accepted 3 February 2006
Available online 21 February 2006

Abstract—The previous exploration of the structure–affinity relationships concerning 4-phenyl-2-quinolinecarboxamide peripheral benzodiazepine receptor (PBR) ligands **6** showed as an interesting result the importance of the presence of a chlorine atom in the methylene carbon at position 3 of the quinoline nucleus. The subnanomolar PBR affinity shown by *N*-benzyl-3-chloromethyl-*N*-methyl-4-phenyl-2-quinolinecarboxamide (**6b**) suggested its chlorine atom to be replaced with other halogens in order to optimize the interaction of the quinolinecarboxamide derivatives with PBR and to develop suitable candidates for positron emission tomography (PET) or single photon emission computed tomography (SPECT) studies. The binding studies led to the discovery of fluoromethyl derivative **6a**, which showed an IC_{50} value of 0.11 nM and is, therefore, one of the most potent PBR ligands so far described. Fluoromethyl derivative **6a** has been labeled with ^{11}C ($t_{1/2}$ = 20.4 min, β^+ = 99.8%) starting from the corresponding des-methyl precursor (**14**) using [^{11}C]CH_3I in the presence of tetrabutylammonium hydroxide in DMF with a 35–40% radiochemical yield (corrected for decay) and 1.5 Ci/μmol of specific radioactivity. Ex vivo rat biodistribution and inhibition (following intravenous pre-administration of PK11195) studies showed that [^{11}C]**6a** rapidly and specifically accumulated in PBR-rich tissues such as heart, lung, kidney, spleen, and adrenal, and at a lower level in other peripheral organs and in the brain. The images obtained in mouse with small animal YAP-(S)PET essentially confirmed the result of the ex vivo biodistribution experiments. The biological data suggest that [^{11}C]**6a** is a promising radioligand for peripheral benzodiazepine receptor PET imaging in vivo.

1. Introduction

The peripheral benzodiazepine receptor (PBR) was originally discovered in the periphery by means of tritium-labeled diazepam and such an important finding stimulated intensive research toward the characterization of this receptor.[1] PBR is mainly localized in peripheral tissues and glial cells. It is highly expressed in steroidogenic tissues such as adrenal gland, but also in kidney, heart, testis and at a lower level in the brain parenchyma, ependyma, choroid plexus, and olfactory neurons. Furthermore, it has been found that PBR is overexpressed in a variety of tumors (e.g., certain brain tumors, ovarian cancer, liver tumors, breast carcinoma, colorectal cancer, etc.) and the PBR expression appears to be related to the tumor malignancy grade.[2] Increased concentrations of PBR were observed in lesioned brain areas in a variety of neuropathologies such as multiple sclerosis, Alzheimer's disease, and Huntington's disease.[3] At a subcellular level, it is mainly localized on the outer mitochondrial membrane even if nonmitochondrial (nuclear or microsomal) localizations in some cells have been suggested. The physiological role of PBR is still unclear, but a wide range of pharmacological

Keywords: Peripheral benzodiazepine receptor; PET; Radiotracer; Synthesis.
* Corresponding author. Tel.: +39 0577 234320; fax: +39 0577 234333; e-mail: cappelli@unisi.it

0968-0896/$ - see front matter © 2006 Elsevier Ltd. All rights reserved.
doi:10.1016/j.bmc.2006.02.004

activities, such as anticonvulsant, anxiolytic, immunomodulating, and cardiovascular, have been related to its activation.[4] In particular, this receptor appears to be involved in steroidogenesis, the regulation of which represents a potential clinical application of PBR ligands.[5] PK11195 (**1**, Fig. 1) was the first non-benzodiazepine ligand which was found both to bind the PBR with nanomolar affinity and to facilitate the transport of cholesterol from the outer to the inner mitochondrial membrane, increasing the rate of pregnenolone synthesis. Isoquinolinecarboxamide derivative **1** is the most widely used pharmacological tool for the study of the expression and the function of PBR (e.g., steroidogenesis and apoptosis). Compound **1** labeled with positron emitter carbon-11 was used in the imaging of brain tumors, multiple sclerosis, cerebral infarction, and abnormalities of calcium channels in heart diseases by means of positron emission tomography (PET).[6]

The class of high affinity PBR ligands also comprises the benzodiazepine Ro5-4864 (**2**) and the imidazopyridine alpidem (**3**), capable of stimulating pregnenolone formation from mitochondria of C6-2B glioma cells.[5] Very recently, the properties of labeled DAA1106 (**4a**: R = $^{11}CH_3$) and its fluoromethyl (**4b**: R = $^{18}FCH_2$) and fluoroethyl (**4c**: R = $^{18}FCH_2CH_2$) derivatives were described and [^{18}F]FEDAA1106 (**4c**) was proposed as a useful PET ligand for PBR which is currently used for the PBR imaging in human brain.[7] Our work culminated in the design and synthesis of potent ligands both in the class of alpidem-related compounds and in the class of PK11195 derivatives[8] as well as in the development of theoretical models for the interaction of PBR with the best known ligands.[9] Again, the quinolinecarboxamide derivatives **5a–c** (**5a**: X = H, R_1 = $CH(CH_3)CH_2CH_3$, R_2 = CH_3; **5b**: X = F, R_1 = $CH(CH_3)CH_2CH_3$, R_2 = CH_3; **5c**: X = H, R_1 = $CH_2C_6H_5$, R_2 = CH_3) were ^{11}C-labeled and the biodistribution studies suggested that these compounds are promising PET tracers for the in vivo imaging of PBR.[10] The evaluation of ^{11}C-labeled **5a-c** in an excitotoxic model of Huntington's disease in rats revealed that benzyl derivative **5c** can be considered an interesting candidate for the in vivo PET monitoring of neurodegenerative processes.[11] The exploration of the structure–affinity relationships (SAFIRs) concerning compounds **6** showed as an interesting result the effect of the presence of a chlorine atom in the methylene carbon at position 3 of the quinoline nucleus.[12] Based on the subnanomolar PBR affinity shown by 3-chloromethyl derivative **6b**, its chlorine atom was replaced by other halogens [e.g., fluorine (**6a**), bromine (**6c**), and iodine (**6d**)] with the aim of optimizing the interaction of the quinolinecarboxamide derivatives with PBR and developing once more better candidates for PET studies. In this paper, we describe the synthesis and the preliminary pharmacological evaluation of a short series of 3-halomethyl-2-quinolinecarboxamide derivatives **6a**,**c**,**d** showing subnanomolar affinity for PBR as well as the radiolabeling with ^{11}C, the results of ex vivo biodistribution and inhibition experiments in rats, and the in vivo PET studies in mice performed on fluoromethyl derivative **6a** to evaluate its potential use as a PET radioligand.

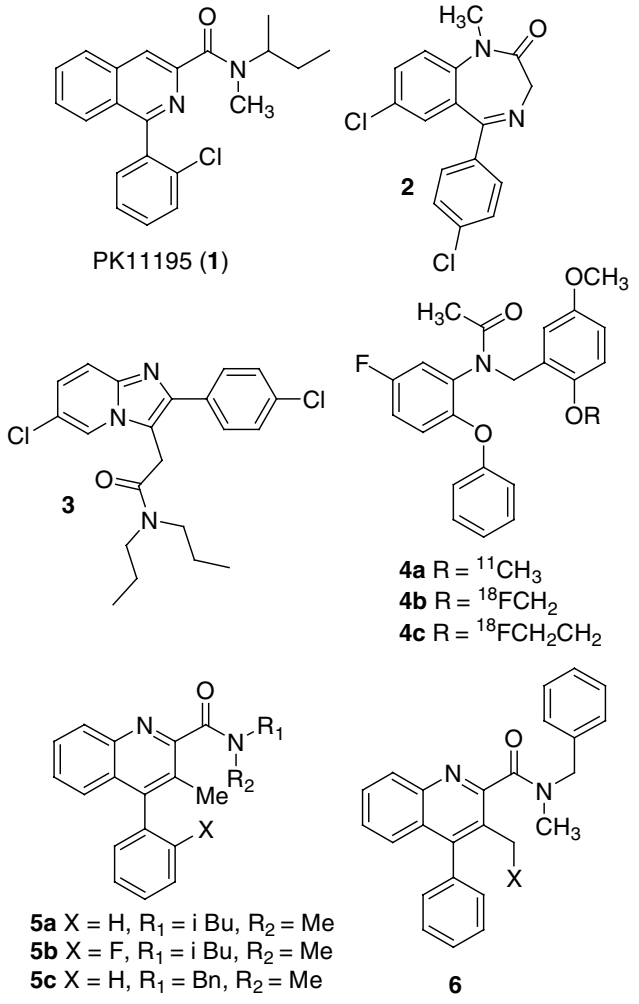

Figure 1. Structure of PBR ligands **1**–**6**.

2. Results

2.1. Chemistry

The previously described quinolinecarboxamide derivatives **5c** and **6b** were re-prepared following the procedure described elsewhere,[12] while new 3-halomethyl-2-quinolinecarboxamide derivatives **6a**,**c**,**d** were synthesized by means of a nucleophilic substitution of the chlorine atom of **6b** with fluoride, bromide, or iodide in the presence of 18-crown-6 (Scheme 1).[13]

In order to obtain the precursor of fluoromethyl derivative **6a** to be used in [^{11}C]CH^3I labeling, a new synthetic procedure was developed in which the fluorine atom was inserted into the molecule in the early steps of the sequence to obtain the fluorinated acid **12** (Scheme 2).

Acid **7**[8b] was converted into ester **9** which was brominated with NBS in the presence of dibenzoyl peroxide to obtain bromomethyl derivative **10**. Nucleophilic substitution of **10** bromine atom with potassium fluoride in

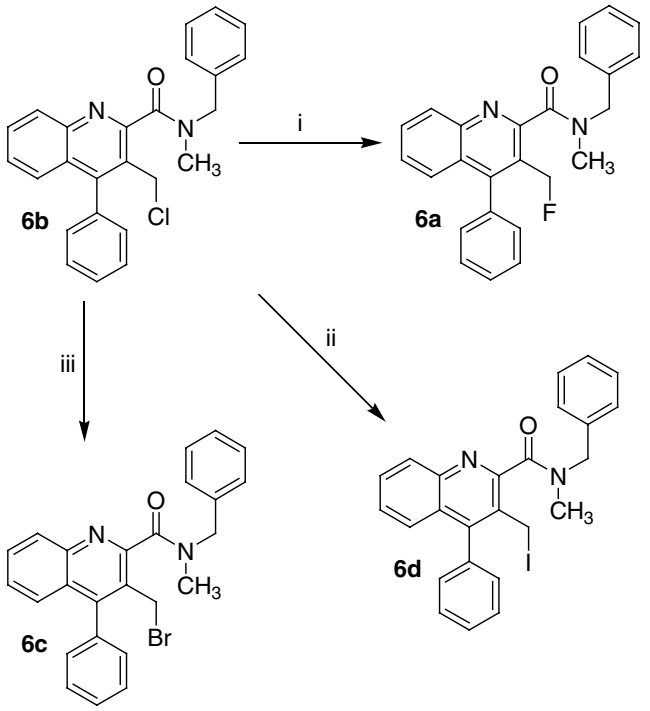

Scheme 1. Reagents: (i) KF, 18-Crown-6, CH_3CN; (ii) NaI, 18-Crown-6, CH_3CN; (iii) LiBr, 18-Crown-6, CH_3CN.

the presence of 18-crown-6 gave ester **11**, which was cleaved with formic acid to afford acid **12**. The acid was converted into the corresponding acid chloride **13**, which was used for the preparation of the secondary amide **14** or the tertiary amide **6a** (Scheme 3). The latter compound was obtained also from the former by methylation with methyl iodide in the presence of sodium hydride as the base. This result demonstrated the feasibility of the labeling of fluoromethyl derivative **6a** with $[^{11}C]CH_3I$.

2.2. Radiosynthesis

Compound [^{11}C]**6a** was synthesized by N–[^{11}C]methylation of the corresponding des-methyl precursor **14** with [^{11}C]methyl iodide in the presence of tetrabutylammonium hydroxide (TBAH) at 80°C for 4 min (Scheme 4) with a radioactivity incorporation yield of 80%. The overall radiosynthesis, including ^{11}C-methylation, HPLC purification and radiopharmaceutical formulation for intravenous administration was completed in an average time of 35 min, from the end of bombardment (EOB) with a 35–40% radiochemical yield (corrected for decay) and 1.5 Ci/μmol of specific radioactivity at the end of radiosynthesis (EOS). In a typical experiment, starting from 900 mCi of $[^{11}C]CO_2$, 100 mCi of [^{11}C]**6a** were obtained with a chemical and radiochemical purity of 100% and over 99%, respectively.

The identity of the final radioactive ^{11}C-radioligand was confirmed by co-injection with the authentic sample of non-radioactive **6a** on reverse-phase high-performance liquid chromatography (HPLC) (see Section 4).

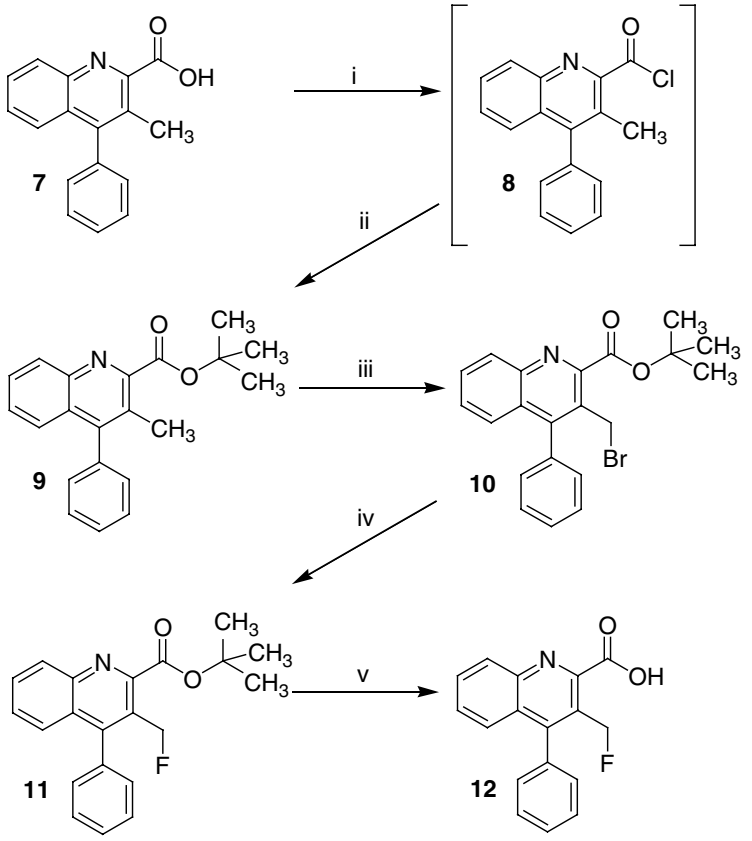

Scheme 2. Reagents: (i) $SOCl_2$, CH_2Cl_2; (ii) *t*-BuOK, THF; (iii) NBS, dibenzoyl peroxide, CCl_4; (iv) KF, 18-Crown-6, CH_3CN; (v) HCOOH.

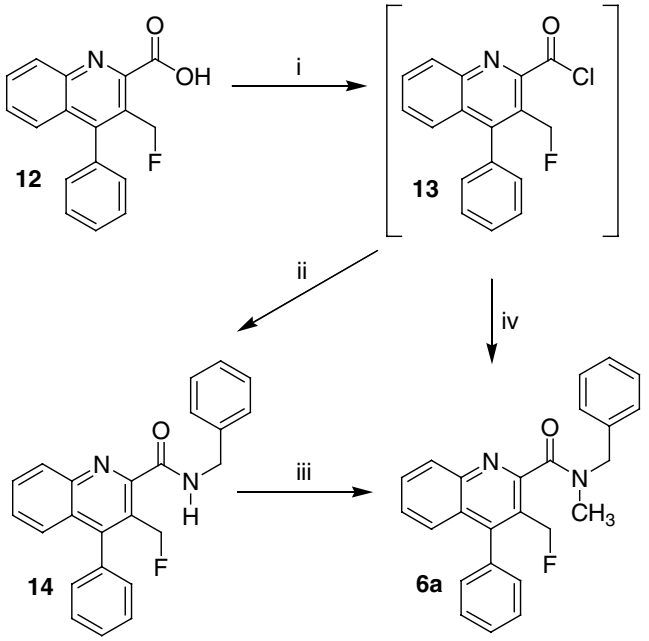

Scheme 3. Reagents: (i) $SOCl_2$, CH_2Cl_2; (ii) $C_6H_5CH_2NH_2$, TEA, CH_2Cl_2; (iii) CH_3I, NaH, DMF; (iv) $C_6H_5CH_2N(CH_3)H$, TEA, CH_2Cl_2.

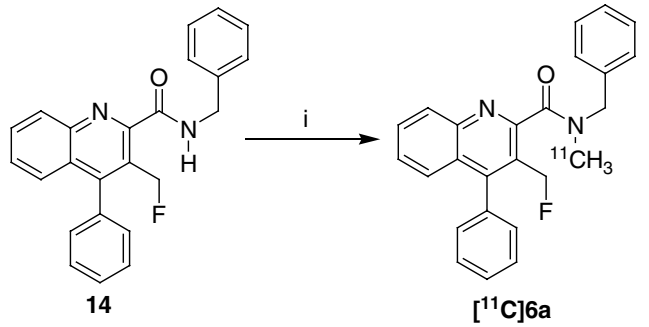

Scheme 4. Reagents: (i) [^{11}C]CH_3I, TBAH, DMF.

2.3. Binding studies

Compounds **6a**–**d** were tested for their potential activity in inhibiting the specific binding of [^{3}H]**1** to rat cortical membrane in comparison with reference compounds **5c** and **1**. The results of the binding studies (Table 1) show that all the 3-halomethyl-2-quinolinecarboxamide derivatives **6a**–**d** display subnanomolar affinity for PBR (IC_{50} values ranging from 0.11 to 0.61 nM). The most potent 3-fluoromethyl derivative **6a** shows an IC_{50} value of 0.11 nM and is about 20 times more potent than reference compound **1**. Thus, 3-fluoromethyl derivative **6a**, being one of the most potent PBR ligands so far described, represents an interesting candidate for radiolabeling with carbon-11 or with fluorine-18 and PET studies. Although slightly less potent, bromomethyl derivative **6c** (IC_{50} = 0.61 nM) can be considered a candidate for radiolabeling with bromine-76 and iodomethyl derivative **6d** (IC_{50} = 0.40 nM) may become a suitable candidate of a SPECT ligand for imaging PBR. The structure–affinity relationship analysis in this short series of highly congeneric PBR ligands confirmed the positive effect of the presence of an halogen atom on the PBR affinity. This 'halogen effect' is particularly evident in the case of fluoromethyl derivative **6a** and appears to correlate with the electron-withdrawing properties of the halogen atom only in the case of compounds **6a**,**b**. If the electron-withdrawing properties are believed to play a role, they may be assumed to activate the methylene hydrogen atoms, which could interact with D157[9] by establishing a non-classical hydrogen bond.[12b] This assumption is considered an interesting working hypothesis for the molecular modeling work, which is in progress in our laboratories.

Table 1. PBR binding affinities of compounds **5c** and **6a–d**

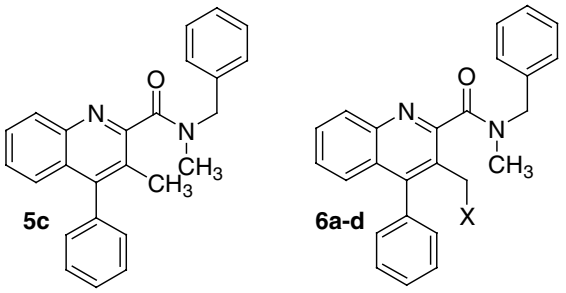

Compound	X	IC_{50} (nM) ± SEM[a]
5c	H	2.1 ± 0.3
6a	F	0.11 ± 0.02
6b	Cl	0.30 ± 0.032
6c	Br	0.61 ± 0.05
6d	I	0.40 ± 0.023
1		2.5 ± 0.4

[a] Each value is the means ± SEM of three determinations and represents the concentration giving half the maximum inhibition of [^{3}H]**1** (final concentration 1 nM) specific binding to rat cortical membranes.

2.4. Kinetic studies

2.4.1. [^{11}C]6a Biodistribution. The tissue biodistribution of [^{11}C]**6a** ([^{11}C]VC701) in albino male CD rats as a function of time is presented in Table 2. As expected, high radioactivity accumulation was observed in peripheral tissues known to be rich in PBR, such as heart, lung, kidney, spleen, and adrenal gland (see Gavish et al.[14] for a review). A lower uptake was observed in other peripheral organs such as intestine, stomach, and liver.

In the remaining tissues, including brain, radioactivity concentration was very low or negligible. In most of the tissues examined, the maximum uptake was reached at 30 min from the injection. At this time, tissue to plasma radioactivity concentration ratios were 2–7 times higher (blood, lung, liver, kidney, spleen, and brain) than the ones previously observed with [^{11}C]**5c**, another PBR ligand developed by our groups (Table 3).[10a] Tissue or blood to plasma ratios of [^{11}C]**6a** remained in general higher than the [^{11}C]**5c** ones also at later times except for blood, liver, adrenal, and testis. A lower interaction with plasma protein may contribute to the higher plasma clearance and tissue to plasma ratios.

Table 2. Cerebral and peripheral distribution of [^{11}C]**6a** in rats[a]

Tissue	10 min	30 min	60 min
Blood	0.038 ± 0.009	0.020 ± 0.007	0.009 ± 0.003
Plasma	0.008 ± 0.002	0.004 ± 0.001	0.008 ± 0.002
Heart	0.459 ± 0.025	0.489 ± 0.048	0.454 ± 0.048
Lung	1.612 ± 0.131	1.023 ± 0.039	0.797 ± 0.017
Stomach	0.100 ± 0.029	0.139 ± 0.004	0.173 ± 0.017
Liver	0.144 ± 0.025	0.103 ± 0.023	0.066 ± 0.002
Adrenal gland	0.390 ± 0.098	0.523 ± 0.000	0.674 ± 0.116
Kidney	0.375 ± 0.045	0.358 ± 0.009	0.334 ± 0.038
Spleen	0.321 ± 0.088	0.487 ± 0.006	0.486 ± 0.025
Testis	0.019 ± 0.002	0.018 ± 0.000	0.020 ± 0.001
Intestine	0.137 ± 0.022	0.174 ± 0.034	0.148 ± 0.035
Muscle	0.062 ± 0.005	0.052 ± 0.009	0.051 ± 0.009
Striatum	0.049 ± 0.005	0.041 ± 0.021	0.011 ± 0.007
Cortex	0.062 ± 0.004	0.039 ± 0.005	0.021 ± 0.006
Cerebellum	0.062 ± 0.004	0.032 ± 0.007	0.015 ± 0.005

[a] Radioactivity concentration is expressed as % of injected dose per gram of tissue (%ID/g). Values are expressed as means ± SD of three rats for each time point.

Table 3. Tissue to plasma ratio of [^{11}C]**6a** and [^{11}C]**5c** in rat at 30 min after the injection[a]

Tissue	[^{11}C]**6a**	[^{11}C]**5c**[b]
Blood	4.49 ± 0.57	1.06 ± 0.09
Heart	112.04 ± 16.15	41.28 ± 11.24
Lung	236.12 ± 47.78	33.51 ± 4.32
Liver	23.28 ± 0.49	7.29 ± 0.63
Adrenal gland	121.24 ± 29.06	44.70 ± 41.71
Kidney	82.71 ± 17.86	17.35 ± 2.84
Spleen	113.15 ± 28.45	24.16 ± 3.63
Testis	4.27 ± 0.95	2.08 ± 0.56
Intestine	39.28 ± 1.71	9.52 ± 3.87
Muscle	11.88 ± 0.74	4.17 ± 1.37
Cerebellum	8.84 ± 1.10	1.98 ± 0.42
Cortex	7.15 ± 0.07	1.57 ± 0.28

[a] The ratio was calculated %ID/g of tissue divided per %ID/g of plasma.

[b] Data of [^{11}C]**5c** were calculated from the results published by Matarrese et al.[10a] Values are expressed as means ± SD of three rats for each time point.

2.4.2. Inhibition study. The specificity of [^{11}C]**6a** in vivo binding to PBR was evaluated in rats pretreated with PK11195 (5 mg/kg, iv, $n = 5$) or with the vehicle (iv, $n = 3$), injected immediately before the radioligand administration. Results of the inhibition experiment at 30 min after [^{11}C]**6a** injection are presented in Figure 2.

The highest effect of PK11195 pre-administration was observed in the heart, lung, kidney, spleen, and stomach (reduction of 86%, 92%, 74%, 87%, and 75%, respectively; $p \leqslant 0.001$). A lower effect was observed in the intestine and in the muscle (52% and 61%, respectively; $\leqslant 0.05$), while no significant inhibitions were observed in blood and brain. Despite the high levels of radioactivity concentration observed in biodistribution experiments, the uptake in the adrenal gland was found to be non-specific as indicated by the absence of PK11195 effect.

2.4.3. PET images. Biodistribution and inhibition images obtained by means of the small animal dedicated tomograph YAP-(S)PET are shown in Figures 3 and 4. In particular, Figure 3 shows a montage of images of radioactivity distribution obtained in a CD-1 mouse injected with [^{11}C]**6a** during the bed 2 of the first acquisition of the study 1 [from 10 to 20 min after the injection, abdomen centered in the field of view (FOV)]. High levels of radioactivity accumulation were observed in the lungs, in the first descending intestinal tract (duodenum), and in the kidneys. Tracer retention was also present in liver, heart, and spleen. No or negligible levels of radioactivity were observed in the brain (bed 1 of the first acquisition in study 1, data not shown) and in the urinary bladder. Thirty minutes after (second acquisition in study 1), no modification in radioactivity distribution was observed. Results of PET images have been confirmed by tissue sampling experiment performed at the end of PET scan in one CD-1 mouse that showed high levels of radioactivity in lungs, intestine and kidney followed by heart, spleen, and liver.

The effect of PK11195 on [^{11}C]**6a** distribution was also evaluated by PET (study 2). Figure 4 shows the radioactivity distribution images obtained at the level of thorax in two CD-1 mice co-injected with vehicle (panel A) or PK11195 (panel B), respectively. Co-injection with PK11195 did not reduce radioactivity accumulation in the small intestine, indicating that tracer retention was not specific (panel B) in this region; on the contrary in agreement with the results of ex vivo inhibition experiments performed in rats, radioactivity uptake was clearly reduced in regions expressing PBRs such as lung, heart, and spleen (panel B).

3. Discussion

The exploration of the structure–affinity relationships of PBR ligands **6** revealed the importance of the presence of a chlorine atom in the methylene carbon at position 3 of the quinoline nucleus.[12] Based on the subnanomolar PBR affinity shown by 3-chloromethyl derivative **6b**, its chlorine atom has been replaced by other halogens (e.g., fluorine, bromine, and iodine) in order to optimize the interaction of the quinolinecarboxamide derivatives with PBR and to develop candidates for PET studies better than the previously described [^{11}C]**5c**.[10a] These studies led to the discovery of fluoromethyl derivative **6a**, which show an IC_{50} value of 0.11 nM (about 20-fold more potent than **1** in the same test system) and can therefore be considered one of the most potent PBR ligands so far described. The properties of fluoromethyl derivative [^{11}C]**6a** as a potential PET radioligand for peripheral benzodiazepine receptor were evaluated ex vivo in rats with biodistribution and inhibition experiments and in vivo in mice with small animal YAP-(S)PET. As expected, in the rat biodistribution, the radioligand rapidly accumulated in PBR-rich tissues such as heart, lung, kidney, spleen, and adrenal, and at a lower level in other peripheral organs and in the brain. The maximum uptake was achieved at 30 min after the iv administration of the tracer, and at this time the specificity of the binding by pre-injecting the isoquinolinecarboxamide derivative PK11195 was investigated. The

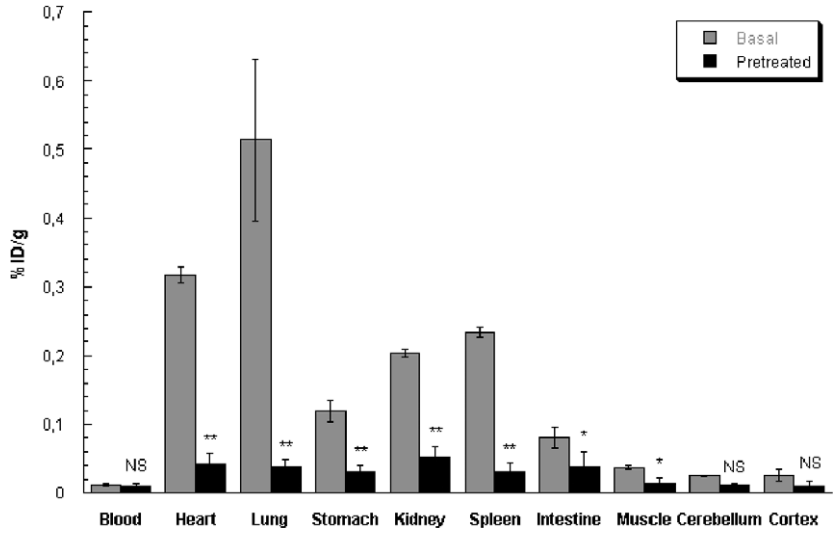

Figure 2. Effect of PK11195 pretreatment on [^{11}C]**6a** radioactivity uptake in cerebral and peripheral tissues of rat measured 30 min after [^{11}C]**6a** injection. Radioactivity concentration is expressed as % of injected dose per gram of tissue (%ID/g); 5 mg/kg of PK11195 (pretreated) or vehicle (basal) was administered immediately before [^{11}C]**6a** injection. Values are expressed as means ± SD of three rats for the basal group and as means ± SD of five rats for pretreated group. Differences between the two groups were examined with Student *t*-test: NS, not significant ($p > 0.05$); *significant ($p \leqslant 0.05$); **very significant ($p \leqslant 0.001$).

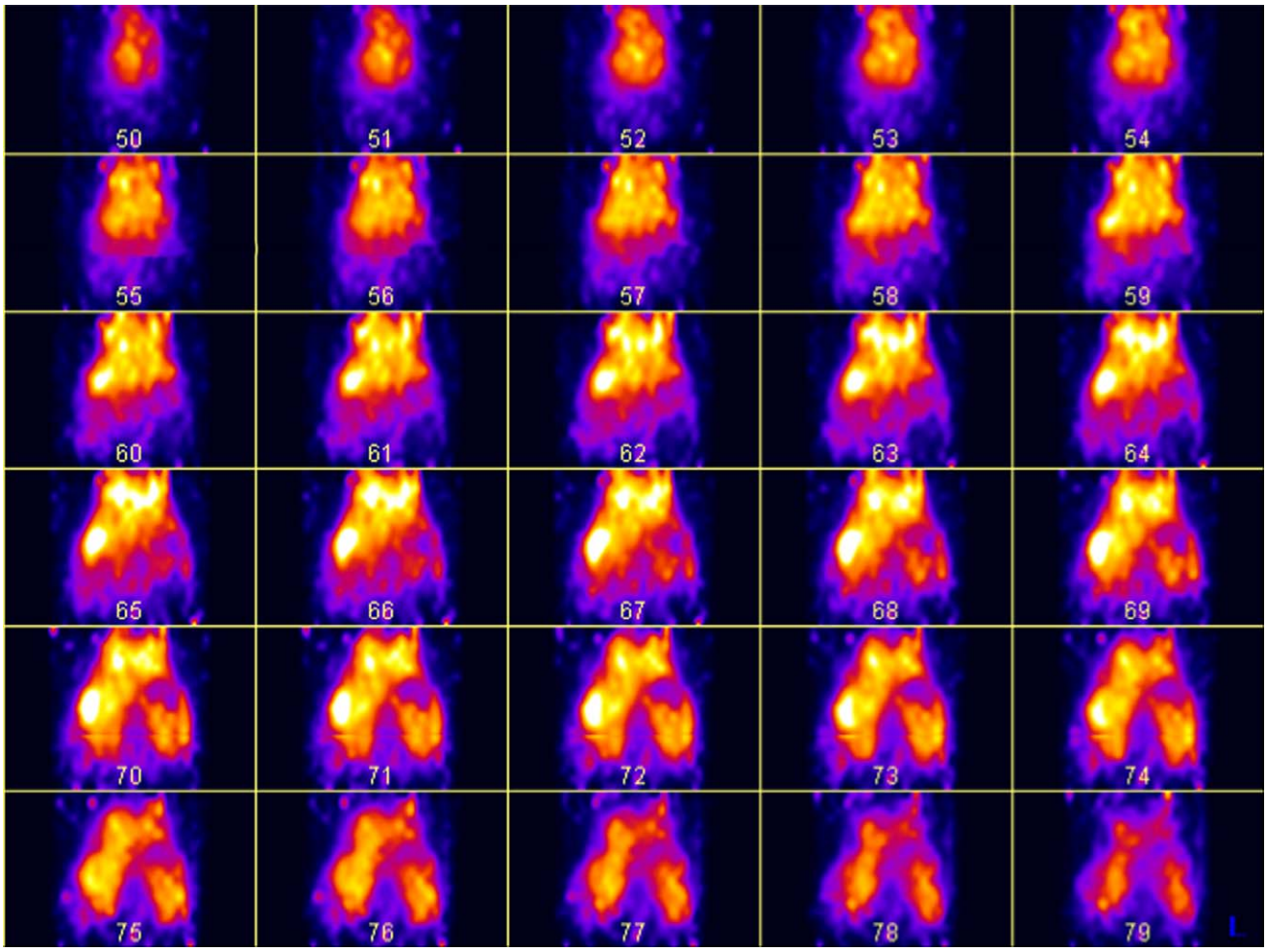

Figure 3. Small animal YAP-(S)PET axial images of CD-1 mice-injected with [^{11}C]**6a**. The animal was acquired prone with the abdomen centred in the FOV starting from 10 min after the tracer injection (bed 2 of the first acquisition of study 1). Numbers refer to the sections and L indicates the left side.

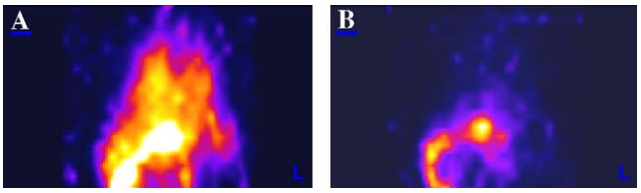

Figure 4. Small animal YAP-(S)PET images (thorax) of two CD-1 mouse injected with [^{11}C]**6a**. One animal was co-injected with the vehicle and acquired after 20 min (A); the other animal was co-injected with the cold compound PK11195 and acquired after 20 min (B).

inhibition experiment demonstrated that the tracer [^{11}C]**6a** specifically binds to PBR in heart, lung, kidney, and spleen, but not in the adrenal. These data disagree with the result obtained for other quinolinecarboxamide derivatives (**5a**–**c**) previously tested,[10a] in which the binding to adrenals was found to be specifically inhibited by pre-injection of PK11195 at the same experimental dose applied. The result can be explained by the higher affinity of **6a** with respect to **5c** and PK11195, that in a region with a very high and clusterized expression of PBR may preclude the observation of any inhibitory effect of PK11195 pre-treatment. Therefore, further inhibition studies with doses of PK11195 or with the cold compound **6a** will be performed to better understand the binding of the tracer in the adrenals. At 30 min after the tracer injection, compound [^{11}C]**5c** (that among the group **5a**–**c** had proved to possess the best pharmacokinetic characteristics) showed a biodistribution profile similar to that of [^{11}C]**6a** in the majority of the organs (Table 3). However, interestingly, the tissue-to-plasma ratios observed with [^{11}C]**6a** were definitely higher than those obtained with [^{11}C]**5c**, suggesting a lower interaction of this compound with plasma proteins, a fact which could be of particular relevance in brain studies on neurodegeneration where new PET ligands with higher signal-to-noise ratios are needed. The value of this tracer for brain studies will be further evaluated and possibly confirmed in selected animal models.

The images obtained in mouse with small animal YAP-(S)PET show that the radiotracer accumulates in lungs, heart, small intestine, and kidneys, and at a lower concentration in spleen and liver. This distribution of the radioactivity was confirmed by our preliminary tissue sampling experiment performed on one mouse at 20 min after the tracer injection (data not shown) and overlapped with the results obtained by Hashimoto et al. in mice injected with [^{3}H]PK11195.[15] The radioactivity uptake in heart, spleen, and liver was masked in the image by the higher signal of the lung and small intestine. The higher uptake found in duodenum was found to be unspecific because it was not inhibited by cold PK11195. No evident binding of the tracer in brain and bladder was detected.

In conclusion, the biological data suggest that [^{11}C]**6a** is a promising radioligand for PBR imaging in vivo with PET showing a higher PBR affinity and better pharmacokinetics features with respect to the previously validated [^{11}C]**5c**.[11] On the basis of these results, compound **6a** will be labeled with the longer-living ^{18}F ($t_{1/2}$ = 109.7 min) and evaluated in both metabolism studies and suitable preclinical models.

4. Experimental

4.1. Chemistry

All chemicals used were of reagent grade. Yields refer to purified products and are not optimized. Melting points were determined in open capillaries on a Gallenkamp apparatus and are uncorrected. Microanalyses were carried out by means of a Perkin-Elmer 240C or a Perkin-Elmer Series II CHNS/O Analyzer 2400. Merck silica gel 60 (230–400 mesh) was used for column chromatography. Merck TLC plates, silica gel 60 F_{254} were used for TLC. ^{1}H NMR spectra were recorded with a Bruker AC 200 spectrometer in the indicated solvents (TMS as internal standard); the values of the chemical shifts are expressed in ppm and the coupling constants (*J*) in hertz. Mass spectra were recorded on either a Varian Saturn 3 spectrometer or a ThermoFinnigan LCQ-Deca.

4.2. 3-Bromomethyl-*N*-methyl-4-phenyl-*N*-(phenylmethyl)quinoline-2-carboxamide (6c)

To a solution of 18-crown-6 (0.023 g, 0.087 mmol) in dry acetonitrile (8.0 mL) was added LiBr (0.22 g, 2.5 mmol) and the resulting mixture was stirred at room temperature for 30 min. To the reaction mixture was added a solution of compound **6b**[12] (0.10 g, 0.25 mmol) in dry acetonitrile (6.0 mL) and the resulting mixture was refluxed under argon for 24 h, poured into ice-water, and extracted with $CHCl_3$. The organic layer was dried over sodium sulfate, and concentrated under reduced pressure. Purification of the residue by flash chromatography with dichloromethane/ethyl acetate (9:1) as the eluent gave pure **6c** as a pale yellow oil (0.070 g, yield 63%). The ^{1}H NMR spectrum of this amide shows the presence of two different rotamers in equilibrium. For the sake of simplification, the integral intensities have not been given. ^{1}H NMR ($CDCl_3$): 2.96 (s), 3.08 (s), 4.47 (s), 4.68 (s), 4.90 (s), 7.30-7.76 (m), 8.10 (m). MS (ESI): *m*/*z* 445 ($M+H^+$). Anal. Calcd for ($C_{25}H_{21}BrN_2O$): C, 67.42; H, 4.75; N, 6.29. Found: C, 67.37; H, 5.04; N, 6.08. R_f, SiO_2 (dichloromethane/ethyl acetate (9:1)): 0.48.

4.3. 3-Iodomethyl-*N*-methyl-4-phenyl-*N*-(phenylmethyl)quinoline-2-carboxamide (6d)

To a solution of 18-crown-6 (0.013 g, 0.049 mmol) in dry acetonitrile (10 mL) was added NaI (0.38 g, 2.5 mmol) and the resulting mixture was stirred at room temperature for 30 min. To the reaction mixture was added a solution of compound **6b**[12] (0.10 g, 0.25 mmol) in dry acetonitrile (8.0 mL) and the resulting mixture was stirred at room temperature under argon for 24 h, poured into ice-water, and extracted with $CHCl_3$. The organic layer was dried over sodium sulfate and concentrated under reduced pressure. Purification of the residue by flash chromatography with dichloromethane/

ethyl acetate (9:1) as the eluent gave pure **6d** as a yellow oil, which slowly crystallized on standing (0.064 g, yield 52%, mp 112–113 °C). The ^{1}H NMR spectrum of this amide shows the presence of two different rotamers in equilibrium. For the sake of simplification, the integral intensities have not been given. ^{1}H NMR ($CDCl_3$): 2.98 (s), 3.09 (s), 4.48 (s), 4.64 (s), 4.90 (s), 7.29–7.74 (m), 8.03 (d, J = 8.3), 8.10 (d, J = 8.3). MS (ESI): m/z 493 ($M+H^+$). Anal. Calcd for ($C_{25}H_{21}IN_2O$): C, 60.99; H, 4.30; N, 5.69. Found: C, 60.80; H, 4.24; N, 5.58. R_f, SiO_2 (dichloromethane/ethyl acetate (9:1)): 0.49.

4.4. 3-Fluoromethyl-*N*-methyl-4-phenyl-*N*-(phenylmethyl)quinoline-2-carboxamide (6a)

4.4.1. Method A. To a solution of 18-crown-6 (5.3 mg, 0.020 mmol) in dry acetonitrile (5.0 mL) was added KF (0.075 g, 1.3 mmol) and the resulting mixture was stirred at room temperature for 30 min. To the reaction mixture was added a solution of compound **6b**[12] (0.090 g, 0.224 mmol) in dry acetonitrile (6.0 mL) and the resulting mixture was refluxed for 14 h, poured into ice-water, and extracted with $CHCl_3$. The organic layer was dried over sodium sulfate and concentrated under reduced pressure. Purification of the residue by flash chromatography with dichloromethane/ethyl acetate (9:1) as the eluent gave pure **6a** as a pale yellow oil, which crystallized on standing (0.035 g, yield 41%). The purification of the residue also gave a mixture of compounds **6b** [R_f, SiO_2 (dichloromethane/ethyl acetate (9:1)): 0.46] and **6a** [R_f, SiO_2 (dichloromethane/ethyl acetate (9:1)): 0.31] on which the above-cited procedure was repeated to obtain further 0.030 g of **6a** (total yield 75%, mp 94–96 °C). The ^{1}H NMR spectrum of this amide shows the presence of two different rotamers in equilibrium. For the sake of simplification, the integral intensities have not been given. ^{1}H NMR ($CDCl_3$): 2.88 (s), 3.08 (s), 4.48 (s), 4.89 (s), 5.44 (d, J = 46.6), 7.29–7.60 (m), 7.74 (m), 8.16 (m). MS (ESI): m/z 407 ($M+Na^+$). Anal. Calcd for ($C_{25}H_{21}FN_2O$): C, 78.10; H, 5.51; N, 7.29. Found: C, 78.23; H, 5.43; N, 7.02.

4.4.2. Method B. A mixture of compound **12** (0.18 g, 0.64 mmol) in CH_2Cl_2 (4 mL) and $SOCl_2$ (4.0 mL) was refluxed for 3 h. Most of $SOCl_2$ was distilled under reduced pressure and the remainder was removed by azeotropic distillation with toluene. The residue was diluted with CH_2Cl_2 (10 mL) and treated in sequence with *N*-benzylmethylamine (0.17 mL, 1.32 mmol) and a solution of triethylamine (0.18 mL, 1.3 mmol) in CH_2Cl_2 (1.0 mL). The reaction mixture was stirred at room temperature for 10 min, diluted with CH_2Cl_2, washed with water, dried over sodium sulfate and concentrated under reduced pressure. Purification of the residue by flash chromatography with petroleum ether/ethyl acetate (8:2) as the eluent gave pure **6a** as a pale yellow, oil which crystallized on standing (0.19 g, yield 77%).

4.4.3. Method C. To a solution of compound **14** (0.036 g, 0.097 mmol) in dry DMF (2.0 mL) with CH_3I (0.30 mL, 4.85 mmol) was added NaH (3.6 mg, 0.15 mmol). The resulting mixture was stirred at room temperature for 1 h, then poured into ice-water and extracted with CH_2Cl_2. The organic layer was washed with water, dried over sodium sulfate, and concentrated under reduced pressure. Purification of the residue by flash chromatography with *n*-hexane/ethyl acetate (8:2) as the eluent gave pure **6a** as a yellow oil (0.036 mg, yield 96%), which crystallized on standing.

4.5. *tert*-Butyl 3-methyl-4-phenylquinolin-2-carboxylate (9)

A mixture of compound **7**[8b] (0.50 g, 1.9 mmol) in CH_2Cl_2 (1.0 mL) and $SOCl_2$ (2.0 mL) was refluxed for 3 h. Most of $SOCl_2$ was distilled under reduced pressure and the remainder was removed by azeotropic distillation with toluene. The residue was treated with a solution of *t*-BuOK (0.30 g, 2.67 mmol) in dry THF (10 mL). The reaction mixture was stirred at room temperature for 1 h, poured into ice-water, and extracted with CH_2Cl_2. The organic layer was dried over sodium sulfate and concentrated under reduced pressure. Purification of the residue by flash chromatography with dichloromethane/ethyl acetate (95:5) as the eluent gave pure **9** as a colorless solid. (0.31 g, yield 51%, mp 146–147 °C). ^{1}H NMR ($CDCl_3$): 1.69 (s, 9H), 2.27 (s, 3H), 7.23–7.67 (m, 8H), 8.17 (d, J = 8.4, 1H). MS (ESI): m/z 342 ($M+Na^+$).

4.6. *tert*-Butyl 3-bromomethyl-4-phenylquinolin-2-carboxylate (10)

A mixture of compound **9** (0.55 g, 1.7 mmol) in CCl_4 (30 mL) with *N*-bromosuccinimide (0.34 g, 1.9 mmol) and dibenzoyl peroxide (0.040 g, 0.165 mmol) was refluxed for 2 h. The reaction mixture was then cooled to room temperature, filtered, and concentrated under reduced pressure. The residue was purified by flash chromatography with dichloromethane as the eluent to give pure **10** as a colorless oil (0.62 g, yield 92%), which crystallized from diethyl ether (colorless prisms, mp 125–127 °C). ^{1}H NMR ($CDCl_3$): 1.77 (s, 9H), 4.68 (s, 2H), 7.32–7.61 (m, 7H) 7.70 (m, 1H), 8.21 (d, J = 8.4,1H). MS (ESI): m/z 420 ($M+Na^+$).

4.7. *tert*-Butyl 3-fluoromethyl-4-phenylquinolin-2-carboxylate (11)

The title compound was obtained from compound **10** (2.1 g, 5.3 mmol) following the procedure described for the preparation of compound **6a** (Method A). Purification of crude **11** by flash chromatography with *n*-hexane/ethyl acetate (8:2) as the eluent gave pure **11** as a white solid (0.70 g, yield 39%, mp 121–123 °C). ^{1}H NMR ($CDCl_3$): 1.71 (s, 9H), 5.43 (d, J = 47.2, 2H), 7.28–7.33 (m,2H), 7.46–7.56 (m, 5H), 7.74 (m, 1H), 8.25 (d, J = 8.3, 1H). MS (ESI): m/z 360 ($M+Na^+$).

4.8. 3-Fluoromethyl-4-phenylquinolin-2-carboxylic acid (12)

A mixture of compound **11** (0.70 g, 2.1 mmol) in formic acid (15 mL) was stirred at room temperature for 20 h. Most of the formic acid was evaporated under reduced pressure and the remainder was removed by azeotropic

distillation with toluene. The resulting residue was treated with diethyl ether to obtain pure **12** as off-white crystals (0.57 g, yield 96%, mp 123–125 °C). ^{1}H NMR ($CDCl_3$): 5.85 (d, $J = 46.2$, 2H), 7.34 (m, 2H), 7.48-7.66 (m, 5H), 7.86 (t, $J = 7.4$, 1H), 8.21 (d, $J = 8.4$, 1H). MS (ESI, negative ions): m/z 280 ($M-H^+$).

4.9. 3-Fluoromethyl-4-phenyl-*N*-(phenylmethyl)quinoline-2-carboxamide (14)

A mixture of compound **12** (0.20 g, 0.71 mmol) in CH_2Cl_2 (4.0 mL) with $SOCl_2$ (4.0 mL) was refluxed for 3 h. Most of $SOCl_2$ was distilled under reduced pressure and the remainder was removed by azeotropic distillation with toluene. The residue was diluted with CH_2Cl_2 (10 mL) and treated in sequence with benzylamine (0.15 mL, 1.4 mmol) and a solution of triethylamine (0.20 mL, 1.4 mmol) in CH_2Cl_2 (1.0 mL). The reaction mixture was stirred at room temperature for 10 min, diluted with CH_2Cl_2, washed with water, dried over sodium sulfate and concentrated under reduced pressure. Purification of the residue by flash chromatography with petroleum ether/ethyl acetate (8:2) as eluent gave pure **14** as a colorless oil (0.18 g, yield 68%), which crystallized from diethyl ether–*n*-hexane to give white crystals melting at 130–132 °C. ^{1}H NMR ($CDCl_3$): 4.75 (d, $J = 6.0$, 2H), 5.88 (d, $J = 46.6$, 2H), 7.29–7.55 (m, 12H), 7.75 (m, 1H), 8.11 (d, $J = 8.5$, 1H), 8.45 (br t, 1H). MS (ESI): m/z 371 ($M+H^+$).

4.10. Radiosynthesis

[^{11}C]Carbon dioxide was produced by the $^{14}N(p,\alpha)^{11}C$ reaction on a IBA Cyclone 18/9 cyclotron, using 18 MeV proton beam at currents 15–30 μA, and trapped in a hollow stainless steel loop, cooled with liquid nitrogen. [^{11}C]Methyl iodide was substantially synthesized as described by Crouzel et al.[16] involving the reduction of [^{11}C]CO_2 with 0.07 M $LiAlH_4$ to lithium aluminum-[^{11}C]methylate, hydrolysis of this intermediate organometallic complex, iodination of the formed [^{11}C]methanol with hydriodic acid, and distillation through an Ascarite–Sicapent purification column. Radiochemical synthesis and purification of [^{11}C]**6a** were performed on the partially modified fully automated synthesis module (PET Tracer Synthesizer, Nuclear Interface Datentechnik GmbH, Münster, Germany) for [^{11}C]-methylation described in detail elsewhere.[17]

High-performance liquid chromatography (HPLC) was performed with a Waters 515 isocratic pump and a Waters 2487 variable-wavelength UV detector in series with a β^+-Bioscan Flow Count detector. Data collection and HPLC control were performed with the use of a Waters Millennium 32 chromatography software package. The course of the ^{11}C-methylation and the quality control of the final radioligand were performed on a reverse-phase analytical HPLC X-Terra RP18, 5 μm, 250 × 4.6 mm, column (Waters). In the analysis of the ^{11}C-labeled compound, unlabeled reference standard **6a** was used for comparison in all the HPLC runs. The pH of the final solution was measured on a Schott Geräte pH-meter. The pyrogenity test was performed using the Limulus Amebocyte Lysate (LAL) test (BioWhittaker, Inc.).

4.11. No-carrier added radiosynthesis of [^{11}C]6a

[^{11}C]Methyl iodide was transported by a stream of argon into the reaction vessel containing 1 mg (0.0027 mmol) of des-methyl precursor **14** in 100 μL DMF containing 1 μL (2 μmol) of tetrabutylammonium hydroxide (60% aqueous solution, Fluka) at 80 °C. After 4 min, the reaction mixture was diluted with 0.8 mL of a solution of acetonitrile/water (1:1; v:v) and injected into the HPLC semi-preparative reverse-phase column. The purification of the tracer was performed by means of an HPLC X-Terra RP18, 250 × 10 mm, 5 μm (Waters) column with CH_3CN:50 mM sodium dihydrogen orthophosphate-1-hydrate (60:40; v:v) at 5 mL/min flow rate with UV detection set at 254 nm. The retention times were 10 min and 8 min for des-methyl precursor **14** and [^{11}C]**6a**, respectively. The retention time of [^{11}C]**6a** was confirmed before each radiosynthesis by comparison with authentic standard of **6a**. The effluent from the column corresponding to [^{11}C]**6a** was collected in 30 mL of sterile water, and the radioligand was recovered by solid-phase extraction (SPE) on pre-activated Sep-Pak C-18 cartridge (Millipore). The Sep-Pak was washed with water (10 mL) before eluting with ethanol (0.5 mL) in a vial containing 9.5 mL of saline solution which was sterilized through a sterile 0.22 μm filter (Gelman Acrodisc). The pH of the final solution was neutral. The quality control of [^{11}C]**6a** was carried out on an analytical HPLC reverse-phase (X-Terra RP18, 5 μm, 250 × 4.6 mm) column (Waters) by means of CH_3CN/25 mM sodium dihydrogen orthophosphate-1-hydrate (75:25; v:v) at 1 mL/min flow rate with monitors for radioactivity and UV detector set at 254 nm. The retention time for [^{11}C]**6a** was 5.4 min. The amount of carrier was calculated from the UV absorbance peak by means of the external standard calibration plot. The minimal detectable concentration of [^{11}C]**6a** was 1.75 nmol/mL.

4.12. In vitro binding assays

Male Sprague–Dawley CD rats (Charles River Italia, Calco, CO, Italy) with body masses of 200–250 g were used. Rats were acclimatized to the new housing conditions for at least one week. They were housed six per cage under an artificial 12-h-light, 12-h-dark cycle at a constant temperature of 22 ± 2 °C, and a relative humidity of 65%. They had free access to water and standard laboratory food at all times. Animal care and handling throughout the experimental procedures were in accordance with the European Communities Council Directive of 24 November, 1986 (86/609/EEC).

Rats were sacrificed by decapitation and their brains were rapidly dissected into the various areas which were stored at −80 °C until the day of the assay. The binding assays were performed as described in the literature.[18] The cerebral cortex was subsequently thawed and then homogenized in 50 volumes of ice-cold Dulbecco's phosphate-buffered saline (PBS), pH 7.4, at 4 °C with

a Polytron PT 10 disrupter (setting 5 for 20 s). The homogenate was centrifuged at 40,000*g* and 4 °C for 30 min and the resulting pellet was resuspended in the same volume of fresh buffer and recentrifuged. The new pellet was resuspended in 10 volumes of the incubation buffer (PBS) and used for the binding assay.

[^{3}H]PK11195 binding was measured in a final volume of 500 μL, consisting of 50 μL membrane suspension (0.15–0.20 mg of protein), 50 μL of [^{3}H]PK11195 (specific activity 85.5 Ci/mmol, New England Nuclear; final assay concentration of 1 nM), 5 μL of drug solution or solvent, and 395 μL PBS. The binding reaction was performed at 25 °C for 90 min and began with the addition of membranes. The incubation was terminated by rapid filtration through glass-fiber filters (Whatman GF/B) which had been presoaked with 0.3% polyethyleneimine and placed in a cell harvester filtration manifold (Brandel). The filters were washed five times with 4 mL of ice-cold PBS, after which filter-bound radioactivity was quantified by liquid scintillation spectrometry. Nonspecific binding was defined as binding in the presence of 10 μM of unlabeled PK11195 (Sigma). Specific binding was determined by subtracting the nonspecific from the total binding and was about 80% of the total binding. The concentration of the test compounds that inhibited [^{3}H]ligand binding by 50% (IC_{50}) was determined by means of Jandel Sigmaplot[19] program with 6–10 concentrations of the displacers, each performed in triplicate.

4.13. Kinetic experiments

4.13.1. Animals. Male albino CD rats (225–250 g; Charles River, Italy) were used for biodistribution and inhibition studies. Male CD-1 mice (35–40 g; Charles River, Italy) were used for small-animal PET imaging. Animal experiments were approved by the Ethical Committee for animal care of the San Raffaele Hospital and carried out in agreement with the Italian and EEC recommendations for the care and use of laboratory animals.

4.13.2. [^{11}C]6a Biodistribution. Compound [^{11}C]**6a** (specific activity at the time of injection: 1.5 Ci/μmol) was diluted to a final volume of 100 μL in saline (0.9% NaCl) and injected into a rat tail vein using a 0.5×9.5 mm syringe needle. The cerebral and peripheral distribution of the radiotracer was assayed at 10, 30, and 60 min ($n = 3$ at each time point) after the injection of approximately 6.3 ± 0.3 MBq of [^{11}C]**6a** (corresponding to 278 ± 12 pmol of cold compound). At the times indicated the animals were sacrificed by decapitation under a light anesthesia (ether) and a blood sample was collected into heparinized tubes, one part of which was counted in a gamma counter and the remaining part was centrifuged for the plasma radioactivity determination. The brain was rapidly removed from the skull and discrete cerebral areas (striatum, cortex, and cerebellum) were dissected out and placed in pre-weighed tubes. The body of the animal was opened and a series of peripheral organs (heart, lung, stomach, liver, adrenal, kidney, spleen, testis, intestine, and muscle) were collected and placed in pre-weighed tubes. The radioactivity was counted in a gamma counter and its concentration calculated as the percentage of injected dose per gram of tissue (%ID/g).

4.13.3. Inhibition study. The specificity of [^{11}C]**6a** uptake (injected dose: 100 ± 9 μCi; specific activity at the time of injection: 2.35 Ci/μmol) was studied in rats pretreated with PK11195 (5 mg/kg dissolved into DMSO/EtOH 1:1, iv, $n = 5$) or vehicle (DMSO/EtOH 1:1, iv, $n = 3$) immediately before the radioligand injection. The inhibitory effect of cold PK11195 was evaluated 30 min after the tracer injection on the basis of our previous experience[10a] and because at this time a maximum radioactivity uptake was found in peripheral organs with high PBR density[20] and was compared to the pre-injection of the vehicle. After this time, the animals were sacrificed by decapitation under a light anesthesia (ether) and processed as described above for the biodistribution to obtain the %ID/g for cerebral and peripheral tissues. The effect of the pretreatment with PK11195 on the [^{11}C]**6a** uptake was expressed as the percentage of inhibition for all the tissues examined and only the tissue with positive percentage is reported.

4.13.4. PET studies. Imaging studies were performed using the YAP-(S)PET scanner (ISE, Pisa, Italy). This small animal tomograph is made up of four detector heads, composed each of a 4×4 cm^2 of $YAlO_3$:Ce matrix of 20×20 elements, $2 \times 2 \times 25$ mm^3 each, coupled to PS-PMT (Hamamatsu R2486). The four modules are positioned on a rotating gantry; opposite detectors are 15 cm apart and in time coincidence when used in PET mode. The scanner has a field of view (FOV) of 4×4 cm of diameter and provides a set of 20 slices of 2 mm thickness. In PET mode, the volume resolution is below 8 mm^3 and is nearly constant over the whole FOV. The maximum absolute sensitivity measured at the center of the FOV is 1.9% (19 cps/KBq) for 50–850 keV energy window.

Two studies were performed on healthy CD-1 mice: in the first study, one animal was acquired in three beds at two different times after the tracer injection; in the second study, two animals were acquired at the level of the thorax starting 20 min after the tracer injection: one animal co-injected with a vehicle (control) and the other co-injected with the inhibitor (inhibited).

Before every study, the mice were anesthetized ip with 800 μL of 1.7% tribromoethanol and positioned supine on the YAP-(S)PET bed.

4.13.5. Study 1. In the first acquisition, the animal was positioned with its head centered in the FOV and was injected into the tail vein with 128 μCi (4.74 MBq) of [^{11}C]**6a**. The acquisition started immediately after the tracer injection. The specific activity calculated at the end of the synthesis was 1.50 Ci/μmol. The first scan was focused on the head (2 time frames of 5 min each), the second scan was focused 4 cm below, at the level of the thorax (2 time frames of 5 min each), and the third scan was focused 4 cm below again, at the level of the abdomen (2 time frames of 5 min each). The data were acquired in list mode using the full axial acceptance

angle of the scanner (3D mode) and then reconstructed with the Expectation Maximization (EM) algorithm.[21]

4.13.6. Study 2. Both the control and the inhibited animals were positioned with the thorax centered in the FOV and acquired 20 min after the tracer injection. The control mouse was injected into the tail vein with 57 μCi (2.11 MBq) of [^{11}C]**6a** and co-injected ip with saline 5% ethanol (vehicle). The inhibited mouse was injected into the tail vein with 25 μCi (0.93 MBq) of [^{11}C]**6a** and co-injected i.p. with 5 mg/kg of the cold compound PK11195 dissolved in DMSO/EtOH (1:1). The specific activity calculated at the end of the synthesis was 6.38 Ci/μmol. For each mouse the thorax was acquired in four time frames of 5 min each. The data were acquired in list mode using the full axial acceptance angle of the scanner (3D mode) and then reconstructed with Expectation Maximization (EM) algorithm.[21]

Acknowledgments

The authors are grateful to Prof. Stefania D'Agata D'Ottavi for the careful reading of the manuscript and to Prof. Alberto Del Guerra and Dr. Antonietta Bartoli (Università degli Studi di Pisa) for assistance in PET acquisition. This work was financially supported by MIUR (Ministero dell'Istruzione, dell'Università e della Ricerca)—PRIN (Programmi di ricerca di Rilevante Interesse Nazionale) and DIMI (Diagnostic Molecular Imaging) Sixth European Program, Project No: LSH-2003-1.2.2.-2.

References and notes

1. (a) Verma, A.; Snyder, S. H. *Annu. Rev. Pharmacol. Toxicol.* **1989**, *29*, 307–322; (b) Saano, V.; Rägo, L.; Räty, M. *Pharmacol. Ther.* **1989**, *41*, 503–514; (d) Gavish, M.; Katz, Y.; Bar-Ami, S.; Weizman, R. *J. Neurochem.* **1992**, *58*, 1589–1601; (d) Beurdeley-Thomas, A.; Miccoli, L.; Oudard, S.; Dutrillaux, B.; Poupon, M. F. *J. Neurooncol.* **2000**, *46*, 45–56.
2. (a) Starosta-Rubinstein, S.; Ciliax, B. J.; Penney, J. B.; McKeever, P.; Young, A. B. *Proc. Natl. Acad. Sci. U.S.A.* **1987**, *84*, 891–895; (b) Black, K. L.; Ikezaki, K.; Toga, A. W. *J. Neurosurg.* **1989**, *71*, 113–118; (c) Black, K. L.; Ikezaki, K.; Santori, E.; Becker, D. P.; Vinters, H. V. *Cancer* **1990**, *65*, 93–97; (d) Miettinen, H.; Kononen, J.; Haapasalo, H.; Helen, P.; Sallinen, P.; Harjuntausta, T.; Helin, H.; Alho, H. *Cancer Res.* **1995**, *55*, 2691–2695; (e) Batra, S.; Iosif, C. S. *Int. J. Oncol.* **1998**, *12*, 1295–1298; (f) Venturini, I.; Alho, H.; Podkletnova, I.; Corsi, L.; Rybnikova, E.; Pellicci, R.; Baraldi, M.; Pelto-Huikko, M.; Helen, P.; Zeneroli, M. L. *Life Sci.* **1999**, *65*, 2223–2231; (g) Hardwick, M.; Fertikh, D.; Culty, M.; Li, H.; Vidic, B.; Papadopoulos, V. *Cancer Res.* **1999**, *59*, 831–842; (h) Maaser, K.; Grabowski, P.; Sutter, A. P.; Hopfner, M.; Foss, H. D.; Stein, H.; Berger, G.; Gavish, M.; Zeitz, M.; Scherubl, H. *Clin. Cancer Res.* **2002**, *8*, 3205–3209.
3. (a) Diorio, D.; Welner, S. A.; Butterworth, R. F.; Meaney, M. J.; Suranyi-Cadotte, B. E. *Neurobiol. Aging* **1991**, *12*, 255–258; (b) Bénavidès, J.; Cornu, P.; Dennis, T.; Dubois, A.; Hauw, J. J.; MacKenzie, E. T.; Sazdovitch, V.; Scatton, B. *Ann. Neurol.* **1988**, *24*, 708–712; (c) Vowinckel, E.; Reutens, D.; Becher, B.; Verge, G.; Evans, A.; Owens, T.; Antel, J. P. *J. Neurosci. Res.* **1997**, *50*, 345–353; (d) Schoemaker, H.; Morelli, M.; Deshmukh, P. *Brain Res.* **1982**, *248*, 396–401.
4. Giesen-Crouse, E. Ed.; In *Peripheral Benzodiazepine Receptors*; Academic Press: London, 1993.
5. Kozikowski, A. P.; Ma, D.; Brewer, J.; Sun, S.; Costa, E.; Romeo, E.; Guidotti, A. *J. Med. Chem.* **1993**, *36*, 2908–2920, and references cited therein.
6. (a) Pike, V. W.; Halldin, C.; Crouzel, C.; Barrè, L.; Nutt, D. J.; Osman, S.; Shah, F.; Turton, D. R.; Waters, S. L. *Nucl. Med. Biol.* **1993**, *20*, 503–525; (b) Junck, L.; Olson, J. M.; Ciliax, B. J.; Koeppe, R. A.; Watkins, G. L.; Jewett, D. M.; McKeever, P. E.; Wieland, D. M.; Kilbourn, M. R.; Starosta-Rubinstein, S.; Mancini, W. R.; Kuhl, D. E.; Greenberg, H. S.; Youngf, A. B. *Ann. Neurol.* **1989**, *26*, 752–758; (c) Pappata, S.; Cornu, P.; Samson, Y.; Prenant, C.; Benavides, J.; Scatton, B.; Crouzel, C.; Hauw, J. J.; Syrota, A. *J. Nucl. Med.* **1991**, *32*, 1608–1610; (d) Junck, L.; Jewett, D. M.; Kilbourn, M. R.; Young, A. B.; Kuhl, D. E. *Neurology* **1990**, *40*, 265; (e) Charbonneau, P.; Syrota, A.; Crouzel, C.; Valois, J. M.; Prenant, C.; Crouzel, M. *Circulation* **1986**, *73*, 476–483.
7. (a) Zhang, M. R.; Kida, T.; Noguchi, J.; Furutsuka, K.; Maeda, J.; Suhara, T.; Suzuki, K. *Nucl. Med. Biol.* **2003**, *30*, 513–519; (b) Zhang, M. R.; Maeda, J.; Ogawa, M.; Noguchi, J.; Ito, T.; Yoshida, Y.; Okauchi, T.; Obayashi, S.; Suhara, T.; Suzuki, K. *J. Med. Chem.* **2004**, *47*, 2228–2235.
8. (a) Anzini, M.; Cappelli, A.; Vomero, S.; Giorgi, G.; Langer, T.; Bruni, G.; Romeo, M. R.; Basile, A. S. *J. Med. Chem.* **1996**, *39*, 4275–4284; (b) Cappelli, A.; Anzini, M.; Vomero, S.; De Benedetti, P. G.; Menziani, M. C.; Giorgi, G.; Manzoni, C. *J. Med. Chem.* **1997**, *40*, 2910–2921.
9. Anzini, M.; Cappelli, A.; Vomero, S.; Seeber, M.; Menziani, M. C.; Langer, T.; Hagen, B.; Manzoni, C.; Bourguignon, J. J. *J. Med. Chem.* **2001**, *44*, 1134–1150.
10. (a) Matarrese, M.; Moresco, R. M.; Cappelli, A.; Anzini, M.; Vomero, S.; Simonelli, P.; Verza, E.; Magni, F.; Sudati, F.; Soloviev, D.; Todde, S.; Carpinelli, A.; Galli Kienle, M.; Fazio, F. *J. Med. Chem.* **2001**, *44*, 579–585; (b) Matarrese, M.; Soloviev, D.; Cappelli, A.; Todde, S.; Moresco, R. M.; Anzini, M.; Vomero, S.; Sudati, F.; Carpinelli, A.; Perugini, F.; Galli Kienle, M.; Fazio, F. *J. Labelled Compd. Radiopharm.* **1999**, *42*, S397–S399.
11. Belloli, S.; Moresco, R. M.; Matarrese, M.; Biella, G.; Sanvito, F.; Simonelli, P.; Turolla, E.; Olivieri, S.; Popoli, P.; Cappelli, A.; Vomero, S.; Galli-Kienle, M.; Fazio, F. *Neurochem. Int.* **2004**, *44*, 433–440.
12. (a) Cappelli, A.; Pericot Mohr, G.; Gallelli, A.; Giuliani, G.; Anzini, M.; Vomero, S.; Fresta, M.; Porcu, P.; Maciocco, E.; Concas, A.; Biggio, G.; Donati, A. *J. Med. Chem.* **2003**, *46*, 3568–3571; (b) Cappelli, A.; Giorgi, G.; Anzini, M.; Vomero, S.; Ristori, S.; Rossi, C.; Donati, A. *Chem. Eur. J.* **2004**, *10*, 3177–3183.
13. More, M. B.; Ray, D.; Armentrout, P. B. *J. Am. Chem. Soc.* **1999**, *121*, 417–423.
14. Gavish, M.; Bachman, I.; Shoukrun, R.; Katz, Y.; Veenman, L.; Weisinger, G.; Weizman, A. *Pharmacol. Rev.* **1999**, *51*, 629–650.
15. Hashimoto, K.; Inoue, O.; Suzuki, K.; Yamasaki, T.; Kojima, M. *Ann. Nucl. Med.* **1989**, *3*, 63–71.
16. Crouzel, C.; Långström, B.; Pike, V. W.; Coenen, H. H. *Appl. Radiat. Isot.* **1987**, *38*, 601–603.

17. Matarrese, M.; Soloviev, D.; Todde, S.; Neutro, F.; Petta, P.; Carpinelli, A.; Brüssermann, M.; Galli Kienle, M.; Fazio, F. *Nucl. Med. Biol.* **2003**, *30*, 79–83.
18. Trapani, G.; Laquintana, V.; Denora, N.; Trapani, A.; Lepedota, A.; Latrofa, A.; Franco, M.; Serra, M.; Pisu, M. G.; Floris, I.; Sanna, E.; Biggio, G.; Liso, G. *J. Med. Chem.* **2005**, *48*, 292–305.
19. Sigma Plot, Jandel Scientific Graphing Software for Windows, San Raphael, CA, USA, 1995.
20. Woods, M. J.; Williams, D. C. *Biochem. Pharm.* **1996**, *52*, 1805–1814.
21. Motta, A.; Damiani, C.; Del Guerra, A.; Di Domenico, G.; Zavattini, G. *Comput. Med. Imaging Graph.* **2002**, *26*, 293–302.